Observation of Arc Start Instability and Spatter Generation in GMAW

Spatter generation due to arc start instability was studied and a temperature model was developed to better understand electrode failure

BY U. ERSOY, S. J. HU, AND E. KANNATEY-ASIBU

ABSTRACT. Arc start instability is a common problem in gas metal arc welding (GMAW) where the arc initially fails to ignite, resulting in low weld penetration and high spatter generation. In this paper, the mechanism of arc start instability is studied using high-speed camera images and sensor data (voltage, current, and wire feed rate), and the spatter generation associated with it is explained in detail. It is shown that the extent of spatter generation due to this instability can be monitored using the voltage and wire feeding rate. An electrode temperature model that incorporates the contact resistance effects at the electrode tip and contact tube is also developed to provide a better understanding of wire disintegration with blunt tip electrodes. It is shown that the contact resistance plays an important role in electrode disintegration.

Introduction

Gas metal arc welding (GMAW) is extensively used in industry for joining sheet metal due to its high productivity and low cost. During GMAW, stable metal transfer is necessary to obtain good-quality welds that are free of spatter and weld bead discontinuity. Arc start instability is a common welding problem during GMAW. If the arc is unable to start successfully, there will be no metal deposition until the arc resumes and excessive spatter will be generated. This will result in low penetration and poor surface quality around the weld.

When the arc fails to start, the electrode comes into contact with the workpiece and heats up as a result of joule heating, followed by electrode wire disintegration. The disintegrated wire pieces fly away from the tip of the electrode and stick to the workpiece as spatter. A significant amount of work exists on spatter analysis during metal transfer in gas metal arc welding (Refs. 1–3). Kang and Rhee (Ref. 1) have developed a model for estimating the amount of spatter in short-circuiting metal transfer mode considering arc extinction. Various waveform (current, voltage) features were used to develop a regression model to estimate the spatter amount. Chen et al. (Ref. 2) explained the mechanism of spatter production in the short-circuiting mode of metal transfer. It is shown that spatter is mainly generated due to CO gas explosion at the instant the short circuit breaks. Kang and Na (Ref. 3) explained the spatter production using the integral of current. The influence of arc current and droplet volume on spatter production was investigated quantitatively. While most models in the literature put more emphasis on the spatter generation during successful modes of metal transfer (globular, spray, short circuiting) due to droplet-weld pool interaction, the mechanism of spatter formation during arc start instability has a different nature compared to such spatter mechanisms since there is practically no weld pool, and the spatter is mostly in the form of solid pieces of electrode wire.

The arc start problem has been studied by Farson et al. (Ref. 4) using high-speed camera imaging and current/voltage signals. The integral of measured current is used as an indication of arc start behavior. It has been shown by a temperature model that during arc initiation, finely pointed tip electrodes disintegrate close to the base metal whereas blunt end tip electrode wires were more likely to disintegrate in the middle section. In the model, the effect of contact resistance at the electrode tip and contact tube was neglected. Incorporating contact resistance effects at the contact tube and workpiece interface enable better understanding of the electrode disintegration.

In this paper, the failure mechanism of arc start in GMAW is studied in detail with the support of high-speed camera imaging and sensor data (voltage, current, and wire feed rate). A spatter index is developed to estimate the amount of spatter generated during the unstable arcing period using voltage and wire feeding rate measurements. In addition, a one-dimensional (1-D) electrode temperature model is developed to estimate the location of electrode wire disintegration by considering the effect of initial contact resistance at the electrode tip and contact tube. Experimental observations of the electrode wire disintegration are in good agreement with model prediction.

KEYWORDS

GMAW
Arc Starting
Spatter Generation
Metal Transfer

Experimental Procedure, Materials, and Equipment

Figure 1 illustrates the general arrangement of the experimental setup. All welding experiments were conducted using the process conditions listed in Table 1 with a stationary weld gun. The welding conditions correspond to a mixed mode of short-circuiting and globular metal transfer. The welding wire material used was AWS ER70S-6 with a diameter of 1.1 mm (0.045 in.) and the workpiece used was ASTM A36M with a thickness of 3 mm (0.12 in.). A Lincoln Power Wave 455 (constant voltage power source) was used during the experiments.

The welding current was measured using a split core Hall effect sensor and the voltage was measured across the contact tube and the workpiece. The wire feed rate was measured using an optical encoder located ahead of the wire feeder motor. Current and voltage were recorded at a sampling rate of 5000 Hz and the wire feed speed was recorded at 100 Hz. The high-speed camera images were recorded at 1000 frames per second with appropri-

U. ERSOY, S. J. HU, and E. KANNATEY-ASIBU are with the Department of Mechanical Engineering, University of Michigan, Ann Arbor, Mich.

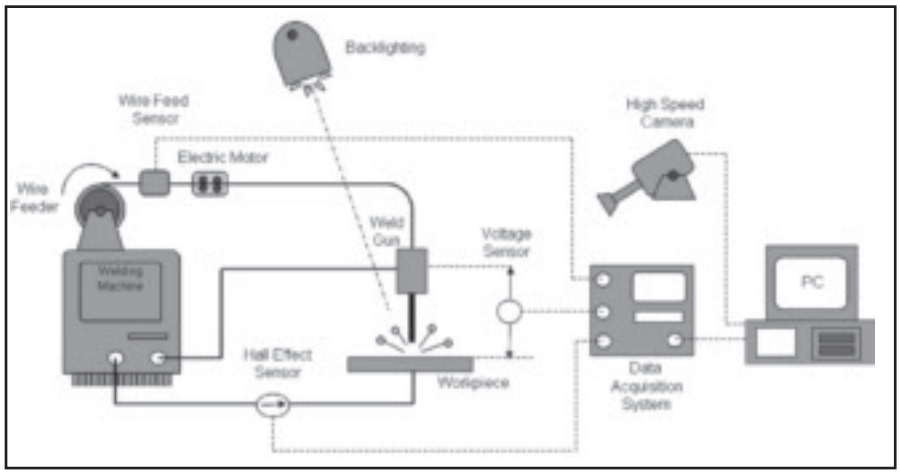

Fig. 1 — Experimental setup.

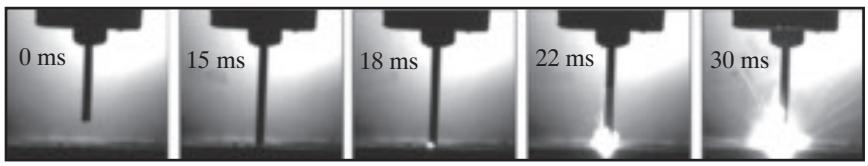

Fig. 2 — Successful arc start.

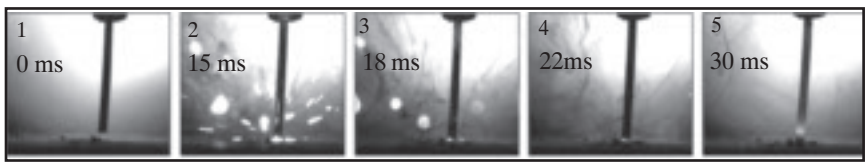

Fig. 3 — Arc start failure.

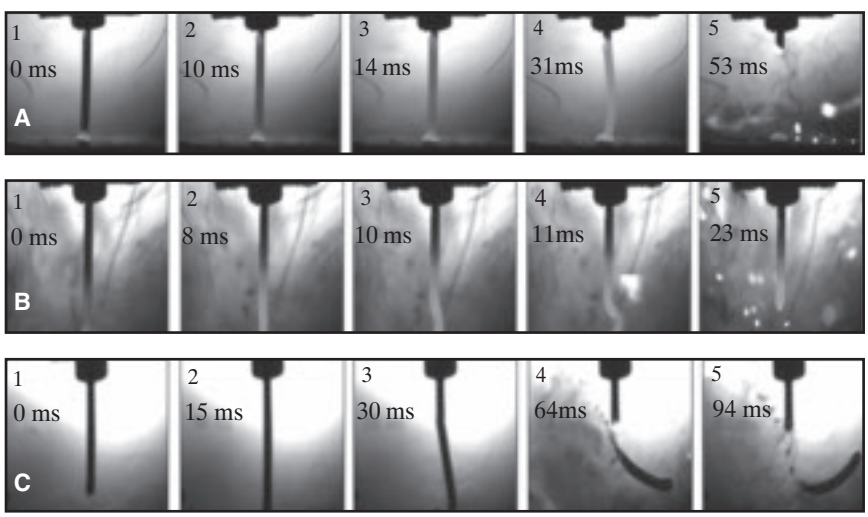

Fig. 4 — Electrode failures. A — Near the contact tube; B — near the tip; C — near the middle section.

ate optical filters and backlighting using a Kodak EktaPro Imager, 1000HR. An ultraviolet filter (Quantaray 52 mm UV) was used with three neutral density filters (Hoya HMC 52 mm NDx4) in series during high-speed imaging. The ultraviolet filter basically absorbs the ultraviolet and blue rays, and the neutral density filters decrease the light intensity. The backlighting was used to capture more details at the boundary of the electrode. Since the experiments were conducted on different days, the setup (backlighting angle, camera location) was subject to variation and not all the high-speed camera images have the same image quality.

Table 1 — Welding Parameters

Voltage	34V
Wire feed rate	340 in./min (8.64 m/min)
Wire diameter	1.1 mm (0.045 in.)
Contact tube-to-work distance	18 mm (0.71 in.)
Shielding gas	100% CO_2

Twenty experiments were conducted that resulted in improper arc starting. The high-speed camera images together with current and voltage signature were recorded simultaneously. The welding wire tip was cut carefully before each experiment so that the tip had a blunt geometry. Spatter was collected by conducting the experiments in a copper box so that all spatter generated was captured. The spatter that stuck to the workpiece was also collected.

Observation of Unstable Arc Start

Under normal welding conditions, the arc starts just after the electrode tip touches the workpiece surface — Fig. 2. As the electrode tip approaches the workpiece, the first spot to make contact is subjected to high current flow. This is accompanied by rupture of asperities. The gas surrounding the spot is superheated and begins to ionize, forming the plasma. Finally, an electric discharge flows through the plasma, which starts the welding arc. As the arc starts, the tip of the electrode wire starts melting and reaches equilibrium at some melting rate. The resulting metal transfer mode is determined by the welding conditions (voltage, wire feeding rate, shielding gas, etc.). If the arc fails to start successfully, the electrode is not melted and comes into contact with the workpiece as a solid wire. Figure 3 shows a series of images for the case when the arc fails to ignite after the first contact. The electrode tip stays in contact with the workpiece along the asperities for some period until the electrode tip thermally welds to the workpiece. Due to excess heat generation, asperity explosions can be observed in Frame 2 of Fig. 3. Asperity softening and melting for stationary contacts was studied in detail by Holm et al. (Ref. 5). It is shown that due to contact softening, the contact asperities move toward each other and finally the current is conducted in solid state.

As the electrode heats up, it disintegrates at some point along its extension.

Based on the twenty experiments with arc start failure, the electrode disintegration took place at three different regions along the electrode extension. Figure 4 shows three different disintegration cases observed during arc welding experiments using the process conditions in Table 1. Thirteen of the experiments resulted in failure near the tip of the contact tube (Fig. 4A), whereas six of them failed near the electrode tip (Fig. 4B). Only one experiment resulted in failure around the middle extension (Fig. 4C). During failure near the contact tube and middle extension, the arc completely extinguished since the welding current was interrupted by an open circuit. It is observed that during tip failure, the arc resumed immediately after disintegration if the electrode tip was close enough to the workpiece.

Arc start instability has a periodic nature in the sense that the electrode wire may experience consecutive breakups until the arc starts successfully. Most of the experiments resulted in multiple electrode wire disintegrations before the arc successfully started. Once the unstable arcing cycle starts, electrode wire disintegration is necessary for the next arc start attempt, otherwise the wire may coil itself on the workpiece, which is undesirable. Arc start failure is accompanied by substantial amounts of spatter due to wire disintegration. In the next section, a spatter index will be studied to estimate the spatter quantity due to unstable arc start using process signature.

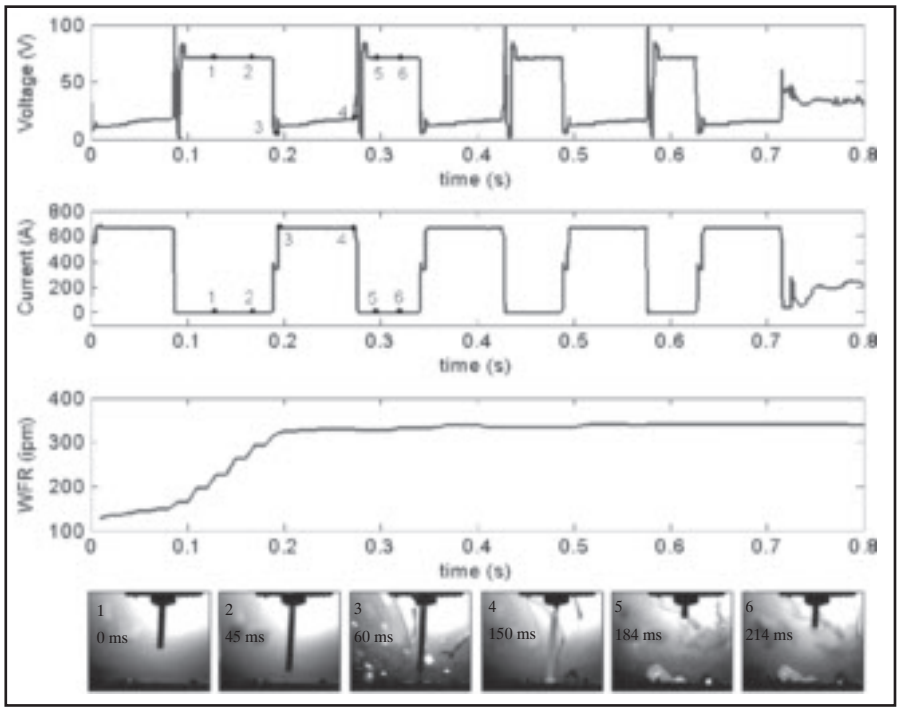

Fig. 5 — Voltage, current, and wire feed rate data synchronized with video images.

Spatter Estimation with Unstable Arc Start

Spatter is defined as particles of molten metal expelled during welding. During the unstable arc start period, the major portion of spatter is in the form of solid pieces and a little portion in the form of molten splashes. The molten splashes are usually generated during the asperity explosion (Fig. 3, Frame 2). They are also observed to emanate from the breakage location during wire disintegration due to high temperatures around these regions (Fig. 4C, Frame 5). The wire pieces generated as a result of an unstable arc start have more potential to contaminate the workpiece surface due to their large size.

Arc start instability can easily be monitored using voltage and current sensors in the welding circuit. Figure 5 shows a typical voltage and current signature from the welding process during the unstable arcing period. Note that the electrode wire experienced four consecutive disintegration events and the high-speed camera images show only the second disintegration event. All four disintegration events occurred near the tip of the contact tube.

As the electrode wire approaches the workpiece, the voltage recorded by the sensor is equal to the open circuit voltage, and the current is zero (Fig. 5, Frames 1, 2). The open circuit duration of the first disintegration event took relatively longer compared to the other three events since the wire feed speed was less than the steady-state value. When the electrode touches the workpiece, the voltage across the electrode first decreases and then gradually increases due to the increasing resistivity of the electrode wire with temperature (Fig. 5, Frames 3, 4).

For failure close to the electrode tip, the voltage and current signature basically follows the same pattern as in Fig. 5, except that the open circuit durations are relatively shorter due to the short length of the disintegrated wire tip.

The spatter amount can be estimated by monitoring the voltage and wire feed rate signature during the unstable arc start period since each jump of the voltage from its low value to the open circuit voltage value corresponds to a piece of wire separating from the electrode material. To quantify the amount of spatter during the unstable arcing period, a spatter index is defined as follows:

$$SI = \pi r^2 \rho \sum_i \bar{u}_i \Delta T_{oc_i} \qquad (1)$$

where r is the electrode radius, ρ is the electrode density, $\bar{u}_i$ is the average wire feed speed, and ΔT_{oci} is the open circuit duration during the i^{th} open circuiting event. Physically, the index is a measure of the total mass of the electrode material lost by the electrode wire disintegration, which is equal to the spatter amount. The mass of broken wire is calculated using the open circuit period, electrode speed, and the wire dimensions and density. A threshold level is used to determine when the open circuiting conditions have been achieved. Note that since the electrode speed is measured before the wire feeder, the interruptions of the wire feeding rate due to electrode contact with the work-

Table 2 — Numbers of Unstable Arc Start Cycles (Open-Circuiting Events)

Measured spatter (g)	0.08	0.087	0.12	0.21	0.26	0.27	0.27	0.31	0.035	0.41	0.49	0.55	0.69	0.71
Predicted spatter (g)	0.21	0.31	0.19	0.24	0.35	0.34	0.46	0.36	0.33	0.65	0.51	0.67	0.72	0.83
No. of open circuits	1	1	1	2	2	2	2	3	3	3	3	4	4	4

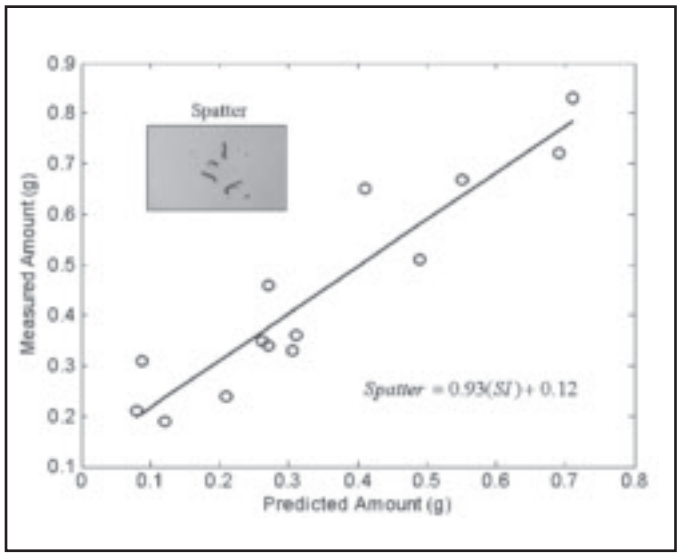

Fig. 6 — Measured vs. predicted spatter amounts.

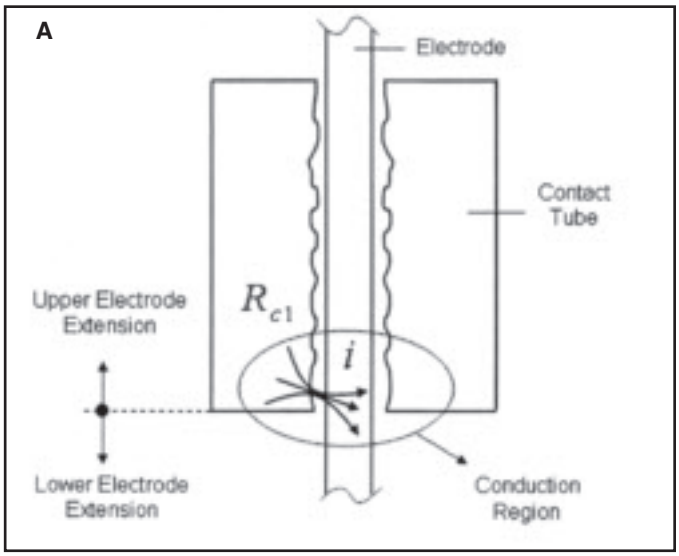

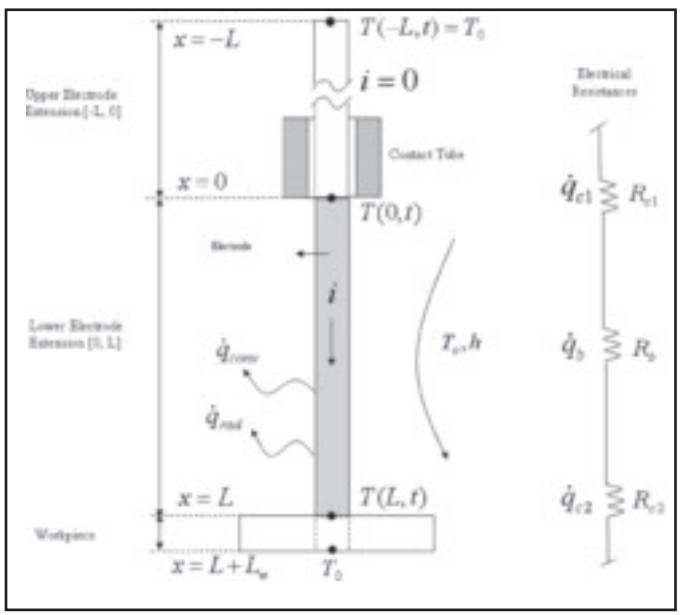

Fig. 8 — Electrode heat transfer model.

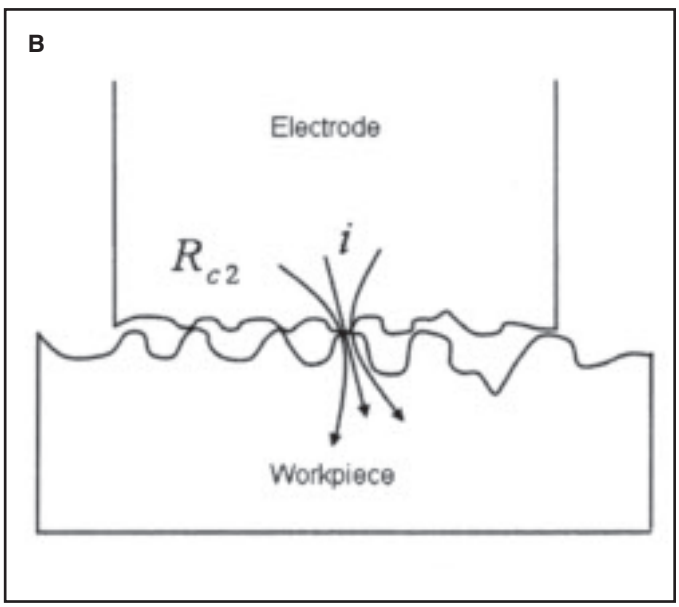

Fig. 7 — Contact resistance due to loose contact at the (A) contact tube, (B) workpiece.

piece are not felt at the measurement point. Therefore, the measured wire feeding rate is not an exact indication of the actual electrode speed at the electrode-workpiece interface and should be used with some reserve.

Figure 6 shows a linear correlation between the measured and the predicted spatter quantity measured during the unstable arcing period. Table 2 lists the number of unstable arc start cycles (open-circuiting events) for each experiment. Note that the total amount of spatter increases as the number of unstable arc cycles and the total duration of the open circuiting events increase. In the next section, a temperature model is presented that incorporates the effect of contact resistance heating to provide a better understanding of different electrode wire disintegration cases observed experimentally.

Electrode Temperature Model

During electrode contact with the workpiece, a high short-circuiting current heats up the electrode. A model for temperature distribution along the electrode is necessary to better understand the electrode disintegration since it is most likely to occur in high-temperature regions on the electrode.

Assumptions

The main assumptions incorporated in the temperature model are as follows:

1) During the electrode contact with the workpiece, the electrode length is assumed to be constant since the electrode comes to a complete stop. Therefore, it is a stationary contact at the electrode-contact tube interface.

2) The electrode is only in contact with the contact tube at its lower tip (Fig. 7A) so that branching of current due to multiple contact points along the upper electrode extension is neglected. The contact tube wear during GMAW was experimentally observed to be maximum at the tip of the contact tube, which supports this assumption (Ref. 6).

3) Contact adherence due to melting at high temperatures is neglected at the

electrode-workpiece and electrode-contact tube interface. Therefore, the contacting surfaces are assumed to have a constant area.

4) The contacting members at the electrode-workpiece and electrode-contact tube have similar resistivities.

5) Heat flow along the electrode is one dimensional.

Governing Equations

The electrode extension between the contact tube and the workpiece, termed lower electrode extension, is heated up by joule heating due to bulk resistance (R_b). The contact resistances at the two ends of the lower electrode extension act as two heat sources. Contact resistance between the electrode and the contact tube (R_{c1}) is due to the loose contact (i.e., clearance gap between the electrode and contact tube) between the two surfaces — Fig. 7A. Similarly, there exists a contact resistance component (R_{c2}) between the electrode and the workpiece after the electrode touches the workpiece surface — Fig. 7B.

By using the configuration in Fig. 8, the governing heat equation is as follows:

$$\frac{\partial^2 T}{\partial x^2}+\frac{\dot{q}}{k}-\frac{hP}{kA_c}\left(T-T_0\right)$$
$$-\frac{\varepsilon\sigma P}{kA_c}\left(T^4-T_0^4\right)=\frac{\rho c_p\left(T\right)}{k}\frac{\partial T}{\partial t} \qquad (2)$$

where $\dot{q}$ is the heat source term due to joule heating, k is the thermal conductivity, h is the convection coefficient, c_p is the specific heat, ρ is the electrode density, ε is the emissivity, σ is the Stefan-Boltzmann constant, P is the electrode perimeter, A_c is the electrode cross section, and T_0 is the room temperature. The current only flows along the lower electrode extension due to the contact conditions. The current along the upper electrode extension is equal to zero due to the assumption of no contact with the contact tube in this region. The upper electrode extension is assumed to be long enough and is set equal to the length of the lower electrode extension so that enough heat can be dissipated. The boundary temperature of the upper electrode extension at $x = -L$ is assumed to be equal to the room temperature. All the heat generated at the electrode-contact tube interface is assumed to be transmitted along the electrode only. The workpiece is assumed to act as a plane wall as an extension of the electrode tip where the temperature below the workpiece ($x = L + L_w$) is assumed to be also equal to room temperature. The $\dot{q}$ term in Equation 2 includes the two contact resistance heating terms at $x = 0$ and $x = L$, respectively, and a bulk resistance heating term along the lower electrode extension. Both the bulk resistance and the contact resistances are functions of temperature. The piecewise joule heating term due to contact and bulk resistance heating is given by the following expression:

$$\dot{q}=\begin{cases} I^2R_{c1}\left(T\right), x=0 \\ I^2R_{c2}\left(T\right), x=L \\ I^2R_b\left(T\right), x\in\left(0,L\right) \end{cases} \qquad (3)$$

The initial and boundary conditions for the electrode column are formulated as follows:

$$T(x,0) = T_0 \qquad (4a)$$

$$T(-L,t)=T_0 \qquad (4b)$$

$$T(L + L_w,t) = T_0 \qquad (4c)$$

The current flowing across the electrode wire does not change much during the electrode contact with the workpiece as can be observed from Fig. 5. The initial and boundary conditions given by Equation 4 only hold for the first electrode contact. If the electrode comes into contact with the workpiece multiple times, then during each additional contact event the electrode has some initial temperature distribution to start with. Therefore, the model does not account for the temperature distribution for additional contacts. The temperature-dependent bulk resistance of the electrode material is often modeled as

$$R_b(T) = R_0[1+ \alpha(T - T_0)] \qquad (5)$$

where R_0 is the resistance at room temperature and α is the temperature coefficient of resistance. R_0 is obtained by measuring the resistance of the electrode wire at room temperature. It is assumed that the electrode has constant asperity density (constant area) at the contact points and the contact resistance is only a function of temperature. By also assuming that the contacting surfaces have similar material properties, the temperature dependence of contact resistances at the contact tube and the workpiece interfaces follow a similar rule as in Equation 5 except that the temperature coefficient of resistance should be modified by a factor of 2/3 (Ref. 7). Therefore, the temperature dependence of contact resistances is modeled as

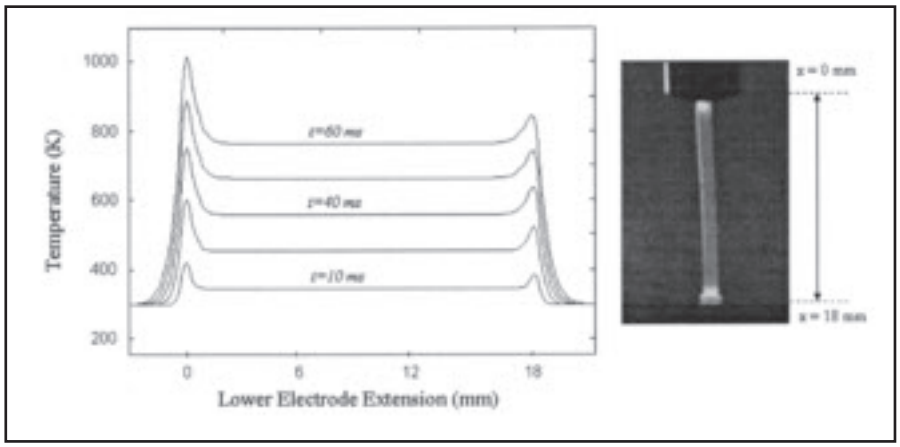

Fig. 9 — Simulation of the electrode temperature distribution along the electrode.

Table 3. — Model Parameters

η	convection heat transfer coefficient	200 W/m^{2}K (35.2 Btu$_{th}$ h^{-1} ft^{-2} °F^{-1})
κ	thermal conductivity	40 W/mK (23.1 Btu$_{it}$ h^{-1} ft^{-1} °F^{-1})
ε	emissivity	0.25 [---]
ρ	density	7850 kg/m^3 (0.28 lb in.$^{-3}$)
α	temperature coefficient of resistivity	3e–3 [°C^{-1}]
σ	Stefan-Boltzmann constant	5.67e-8 W/m^{2}K^4 (1.714 × 10^{-9} Btu/h-ft^2 - °R^4
c_p	specific heat capacity	121+0.85T[J/kgK] (1 J/kgK =2.39e-4 Btu$_{th}$ lb^{-1} °F^{-1}
T_0	room temperature	298 K (77°F)
R_0	room temperature bulk resistance	75[mΩ]
R_{01}	contact resistance (contact tube) at T_o	40[mΩ]
R_{02}	contact resistance (electrode tip) at T_o	27[mΩ]

$$R_{ci}(T) = R_{0i}(1 + 2/3\alpha(T-T_0)) \qquad (6)$$

where R_{ci} denotes the contact resistance, whereas R_{0i} is the room temperature contact resistance for the contacting surfaces (i = {1,2}).

Measurement of Contact Resistances at Room Temperature

The room temperature contact resistances at the contact tube (R_{01}) and workpiece (R_{02}) were experimentally measured by a 4-wire Kelvin method. The measured resistance between the electrode and workpiece ranged between 16 and 40 $m\Omega$ for blunt electrode tips. The resistance value between the electrode and contact tube is highly dependent on the clearance gap between the two surfaces. For new contact tubes where the gap between the electrode and contact tube was small, the contact resistance measurements ranged between 14 and 60 $m\Omega$, whereas for worn-out contact tubes, it ranged between 150 and 200 $m\Omega$. The dependence of contact tube wear on contact resistance in GMAW has been studied by Zwickert and Krupp (Ref. 8). It was shown that the contact resistance at the contact tube increases as the electrode wears. It should be noted that different contact tubes and electrode materials will result in different contact resistance values at room temperature.

Simulation Results

Equation 2 was solved using Matlab with 100 time steps and 200 mesh points in the spatial coordinate. The parameters used in the heat equation are summarized in Table 3. The solution method (spatial discretization of parabolic equations) is explained in Ref. 9. The effect of heat lost by convection and radiation on the temperature distribution was negligible compared to joule heating. Figure 9 shows an example simulation result for temperature distribution along the lower electrode extension in the early stages after the electrode contact with the workpiece.

The upper electrode extension and the workpiece act as a heat sink, so the temperature has a steep gradient at the boundaries of the lower electrode extension. The room temperature contact resistance at the electrode-contact tube interface was chosen as the average of the measured values for a new contact tube free of wear. Although the temperature distribution along the electrode during the actual welding process could not be measured, it is obvious from the color intensity of the image (Fig. 9) that the electrode is hotter at the electrode tip and in the vicinity of the contact tube, which supports the model. The color intensity in the middle portion of the electrode is uniform indicating that the temperature is fairly constant as predicted by the simulation. Note that different electrode contact conditions (surface film, greasy surface, etc.) may result in variation of the temperature level in the contact regions.

The simulation results indicate that disintegration is most likely to take place at the boundaries of the lower electrode extension since melting will first start around these regions due to high temperatures. The simulation results appear to be in good agreement with the high-speed camera observations. As mentioned previously, more than half of the experiments resulted in failure at the tip of the contact tube (Fig. 4A), whereas all but one of the rest had failure at the tip of the electrode (Fig. 4B). Middle section failure was observed only in one case (Fig. 4C). The contact resistance values at the two ends of the electrode play a key role in determining where the disintegration will take place since melting first starts in these regions.

For contact tubes with poor electrical conductivity due to wear and contamination during service, the electrode wire disintegration will most likely occur near the contact tube due to higher contact resistance compared with the electrode tip. For pointed tip electrodes, the electrode tip-workpiece contact resistance is expected to exceed the contact tube-electrode contact resistance, in which case the model will predict hotter spots at the electrode tip. It's believed that the disintegration may occur around the middle section due to coupled mechanical effects due to buckling, which was not studied in this paper.

Conclusions

In this paper, the mechanism of unstable arcing due to arc start instability and its effect on spatter generation was studied. Unstable arc start can generate substantial amount of spatter depending on the electrode disintegration location as revealed by high-speed camera images. It is shown that the amount of spatter generated is directly proportional to the duration of this instability (i.e., duration of open circuiting events).

Methods are developed to monitor the unstable arcing period using the process signature and to estimate the spatter quantity associated with this instability. A temperature model that includes the effect of contact resistance is also used to enhance our understanding of the electrode wire disintegration.

It is shown that during electrode contact with the workpiece, melting first starts at the boundaries of the lower electrode extension due to the high temperatures in these regions, as a result of contact resistance. Consequently, during arc start instability the electrodes mostly disintegrate close to the contact tube and the electrode tip.

Acknowledgments

This research was supported by the General Motors Collaborative Research Laboratory at the University of Michigan.

References

1. Kang, M. J., and Rhee, S. 2001. The statistical models for estimating the amount of spatter in the short circuit transfer mode of GMAW. *Welding Journal* 80(1): 1-s to 8-s.

2. Chen, J. H., Sun, Z. C., and Fan, D. 1996. Study on the mechanism of spatter produced by basic welding electrodes. *Welding Journal* 75(10): 312-s to 316-s.

3. Kang, S. K., and Na, S. J. 2005. A mechanism of spatter production from the viewpoint of the integral of specific current action. *Welding Journal* 84(12): 188-s to 196-s.

4. Farson, D., Conrardy, C., Talkington, J., Baker, K., Kerschbaumer, T., and Edwards, P. 1998. Arc initiation in gas metal arc welding. *Welding Journal* 77(8): 315-s to 321-s.

5. Holm, E., and Holm, R. 1953. The fundamentals of the welding of electric contacts under heavy current conditions. ASTM Bulletin, No. 188, pp. 39–44.

6. Quinn, T. P., Madigan, R. B., Mornis, M. A., and Siewert, T. A. 1995. Contact tube wear detection in gas metal arc welding. *Welding Journal* 74(4): 115-s to 121-s.

7. Holm, R. 1958. *Electric Contacts Handbook.* pp. 78–85, Berlin, Springer-Verlag.

8. Zwickert, H., and Krupp, W. 1984. On the electrical current transfer between the contact tube and the welding wire in MIG/MAG welding. *Schweisstechnick* (Berlin) 34(8): 348–350.

9. Skeel, R. D., and Berzins, M. 1990. A method for the spatial discretization of parabolic equations in one space variable. *Siam J. Sci. Stat. Comput.* 11(1): 1–32.